Satellite-driven modelling of NO2 and PM2.5 across Germany (2019–2024): a multi-sensor machine-learning approach

Rebecca Miller, Jonas Olbrich, Wierer Manuel, Jia Chen, Michael Wurm, Cesar Ivan Alvarez

Angaben zur Veröffentlichung / Publication details:

Miller, Rebecca, Jonas Olbrich, Wierer Manuel, Jia Chen, Michael Wurm, and Cesar Ivan Alvarez. 2026. "Satellite-driven modelling of NO2 and PM2.5 across Germany (2019–2024): a multi-sensor machine-learning approach." *Environmental Pollution* 396: 127898. https://doi.org/10.1016/j.envpol.2026.127898.

Environmental Pollution 396 (2026) 127898

Contents lists available at ScienceDirect

Environmental Pollution

journal homepage: www.elsevier.com/locate/envpol

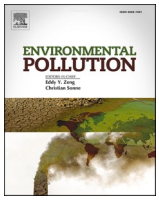

Satellite-driven modelling of NO_2 and $PM_{2.5}$ across Germany (2019–2024): A multi-sensor machine-learning approach

Rebecca Miller [a], Jonas Olbrich [a], Wierer Manuel [a], Jia Chen [b], Michael Wurm [c], Cesar Ivan Alvarez [a,*]

[a] University of Augsburg, Universitätsstrasse 12a, 86159, Augsburg, Germany
[b] Chair of Environmental Sensing and Modeling, Technical University of Munich, Munich, 80333, Germany
[c] German Aerospace Center (DLR), Earth Observation Center (EOC), Oberpfaffenhofen, 82234, Germany

ARTICLE INFO

Keywords:
Germany
Remote sensing
Air pollution
NO2
PM2.5
Machine learning
Google earth engine

ABSTRACT

Mapping air pollution across space remains challenging, even in countries with dense monitoring networks. In Germany, pollutant levels can change over short distances because of traffic, land use, and meteorological conditions, while national assessments often rely on unevenly distributed monitoring stations. This study examines how openly available satellite observations and reanalysis data can support annual modelling of NO_2 and $PM_{2.5}$ across Germany from 2019 to 2024. Sentinel-5P (NO_2 and CO), MODIS Normalized Difference Vegetation Index (NDVI) and Multi-Angle Implementation of Atmospheric Correction (MAIAC) aerosol optical depth (AOD), and ERA5-Land meteorological variables were combined with EuroAirnet observations, and seven machine-learning algorithms were evaluated. Model performance was assessed using random cross-validation, an independent test set, and spatial cross-validation, while SHAP (Shapley Additive Explanations) values were used to interpret predictor contributions. For NO_2, Random Forest achieved the highest accuracy ($R^2 = 0.68$; RMSE = 5.87 μg m^{-3}), with SHAP analysis identifying tropospheric NO_2 and vegetation structure (NDVI) as the most influential predictors. $PM_{2.5}$ proved more difficult to model at the annual scale: Gradient Boosting performed best ($R^2 = 0.50$; RMSE = 11.53 μg m^{-3}), with surface pressure, NDVI, and co-emitted gases emerging as key variables, while MAIAC AOD contributed little independent information when aggregated annually. A sensitivity analysis showed that including a static road-density layer improved NO_2 estimates near monitoring sites but provided limited gains under spatial validation. The resulting concentration maps reproduce the main national patterns observed in the monitoring network, showing a decline in NO_2 and more regionally variable behaviour for $PM_{2.5}$. Although annual predictors cannot capture short-term variability or highly localised emission sources, the study provides a transparent and reproducible framework for national-scale air-quality assessment based entirely on open global datasets and highlights the potential to integrate additional Earth observation and climate reanalysis products in future research.

1. Introduction

Nitrogen dioxide (NO_2) and fine particulate matter ($PM_{2.5}$) remain two of the most closely monitored air pollutants in Europe because of their well-established links to human health (World Health Organization, 2025). Despite more than three decades of air-quality policies, concentrations in many urban and industrial areas continue to exceed recommended limits. In Germany, road traffic—particularly diesel passenger cars and light-duty vehicles—remains the largest contributor to NO_x emissions, accounting for nearly 60% of national transport-related NO_x in 2022 (UBA, 2024). $PM_{2.5}$, by contrast, arises from a more complex mixture of sources. As exhaust-after-treatment technologies have improved, secondary aerosol formation driven by agricultural ammonia, industrial emissions, and residential wood burning has become increasingly important (EEA, 2023). These diverse contributions, together with meteorological and seasonal influences, create strong spatial and temporal gradients in air-pollution levels (Rackow et al., 2025).

* Corresponding author. Universität Augsburg, Universitätsstraße 12, 86159, Augsburg, Germany.
E-mail addresses: rebecca.miller@uni-a.de (R. Miller), jonas.olbrich@uni-a.de (J. Olbrich), manuel.wierer@uni-a.de (W. Manuel), jia.chen@tum.de (J. Chen), Michael.Wurm@dlr.de (M. Wurm), cesar.alvarez@uni-a.de (C.I. Alvarez).

https://doi.org/10.1016/j.envpol.2026.127898
Received 8 January 2026; Received in revised form 12 February 2026; Accepted 26 February 2026
Available online 28 February 2026

The health implications of this variability are significant. Long-term exposure to NO_2 and $PM_{2.5}$ is associated with increased risks of cardiovascular disease, stroke, and premature mortality (Wang et al., 2025), even at levels below current EU limit values (WHO, 2021). In Germany, ambient $PM_{2.5}$ exposure caused an estimated 27,040 premature deaths in 2019 (Hahad et al., 2025), and for 2022, approximately 32,600 deaths were attributable to $PM_{2.5}$ and 9400 to NO_2. Across the EU-27, more than 80% of the urban population remains exposed to concentrations above WHO guideline levels (EEA, 2024). Although population-weighted $PM_{2.5}$ exposure in Germany has fallen by 54% since 2010 (UBA, 2025), average concentrations still exceed the updated WHO guideline of 5 μg m^{-3} for most residents. These patterns highlight both the progress achieved and the persistent need for more spatially resolved exposure assessments to support environmental-health protection.

Germany operates one of the densest air-quality monitoring networks in Europe, yet even such extensive systems cannot fully capture the rapid spatial changes in pollutant concentrations that occur within cities or across heterogeneous landscapes. Air quality can vary substantially over just a few hundred meters due to traffic flows, street canyons, meteorological conditions, and neighbouring land-use patterns (Essamlali et al., 2025). As cities expand and reorganise, the configuration of the urban environment itself shapes pollution distributions—an effect highlighted by Wurm et al. (2025), who show that how "urban" areas are defined strongly influences observed exposure patterns. Moreover, as Alvarez-Mendoza et al. (2019) note, relying only on fixed stations leaves important gaps, especially in areas with fewer sensors. Addressing these gaps requires complementary approaches that can better capture the fine-scale spatial complexity of air-pollution exposure.

Satellite remote sensing helps overcome these limitations by providing continuous, country-wide observations of atmospheric and land-surface processes (Alvarez et al., 2026). Remote sensing—based on measuring reflected or emitted electromagnetic radiation (Stratoulias et al., 2024)—enables consistent monitoring of air-quality-relevant variables across space and time. Sentinel-5P ffers daily tropospheric NO_2 retrievals (European Space Agency, 2018), while Moderate-Resolution Imaging Spectroradiometer (MODIS) products such as Normalized Difference Vegetation Index (NDVI) (Didan, 2021) and Multi-Angle Implementation of Atmospheric Correction (MAIAC) aerosol optical depth (Lyapustin & Wang, 2018) capture vegetation structure and aerosol distributions that influence pollutant levels. When combined with meteorological reanalysis data, these datasets provide information on boundary-layer dynamics, stagnation events, and secondary aerosol formation—meteorological processes known to be strong predictors of NO_2 and $PM_{2.5}$ (Zhang et al., 2018).

Recent advances in machine learning have further strengthened the use of satellite data for air-quality estimation (Chauhan et al., 2021; Anggraini et al., 2024, 2025). A growing number of studies show that integrating remote sensing, meteorology, and ground observations can yield accurate, spatially continuous pollution estimates. For example, Balamurugan et al. (2023) mapped near-surface NO_2 and O_3 across Germany using Sentinel-5P in a machine-learning framework, while Janhäll (2015) demonstrated that Random Forest models can effectively translate Aerosol optical depth (AOD) information into $PM_{2.5}$ estimates. A recent review by Lolli (2025) emphasises that machine-learning-based satellite fusion is becoming one of the most scalable and effective approaches for surface air-quality assessment, particularly in regions with limited monitoring infrastructure.

Despite these advances, several gaps remain. First, most national-scale air-quality studies in Europe focus on short-term or daily modelling, while fewer studies systematically evaluate annual exposure patterns using fully open and reproducible Earth Observation workflows. Second, many modelling frameworks rely on proprietary emission inventories, locally derived land-use data, or region-specific predictors that limit transferability and comparability across countries. Third, limited attention has been given to evaluating model interpretability and physical consistency using explainable machine-learning approaches at national scale. In the case of Germany, although monitoring networks are dense, uneven station distribution and strong intra-urban variability still create spatial gaps in exposure representation. A transparent modelling framework that integrates satellite observations, climate reanalysis, and ground measurements using exclusively open datasets remains methodologically and policy relevant.

In addition to addressing these methodological gaps, the selection of an annual temporal scale is deliberate. Annual concentration metrics are directly aligned with regulatory limit values and long-term health exposure assessments, which are typically defined on an annual basis. Aggregating predictors to annual medians reduces short-term meteorological variability, episodic pollution peaks, and retrieval noise in satellite observations, thereby improving the stability of predictor–response relationships in national-scale models. Moreover, Sentinel-5P provides observations at a fixed daily overpass time, limiting representation of diurnal variability; annual aggregation therefore offers a temporally consistent framework for integrating satellite and ground-based data. For these reasons, the present study prioritises annual exposure patterns to provide a robust representation of spatial gradients across Germany.

Building on this context, this study examines how open satellite observations and high-precision ground measurements can be combined to better characterise air quality across Germany from 2019 to 2024. Using Sentinel-5P NO_2, MODIS vegetation and aerosol products, and ERA5-Land meteorology, we explore spatial and temporal patterns of NO_2 and $PM_{2.5}$ while addressing known challenges related to spatial variability and station coverage. This integrated framework provides a more complete picture of air-pollution dynamics, supports exposure assessment in under-monitored regions, and contributes evidence relevant to ongoing discussions around EU air-quality standards and updated WHO guidelines.

2. Materials and methods

2.1. Germany in terms of air pollution

Germany is in Central Europe at approximately 51° N and 10° E (Fig. 1). Historically, the country has experienced relatively high air-pollution levels compared with other European nations, although emissions have declined over recent decades following the implementation of ambitious climate and clean-air policies (OECD, 2023). Current pollution sources are dominated by road traffic, combustion processes, industrial and commercial activities, and emissions from private households (Kessinger et al., 2025).

From the early 2000s to the mid-2010s, concentrations of $PM_{2.5}$ and NO_2 showed substantial variability, and exceedances of EU limit values were common (European Parliament & Council of the EU, 2008). In 2010, more than 70% of traffic-oriented urban stations exceeded the annual NO_2 limit of 40 μg m^{-3}, whereas by 2020 this share had dropped below 5%, partly due to reduced emissions during COVID-19 lockdowns (Schatke et al., 2022). In 2024, EU limit values for NO_2 and $PM_{2.5}$ were met nationwide for the first time. However, exceedances remain widespread when applying the stricter WHO guidelines, with 97% of stations exceeding the NO_2 guideline (10 μg m^{-3}) and 74% exceeding the $PM_{2.5}$ guideline (5 μg m^{-3}) (WHO, 2024). These findings highlight the continued challenge of meeting health-based standards (Heinrich et al., 2002) and the need for spatially detailed assessments to identify remaining pollution hotspots.

2.2. Data and methods

2.2.1. Ground data from the European air-quality monitoring network (EuroAirnet)

For this study, ground-based air-quality data were obtained from the

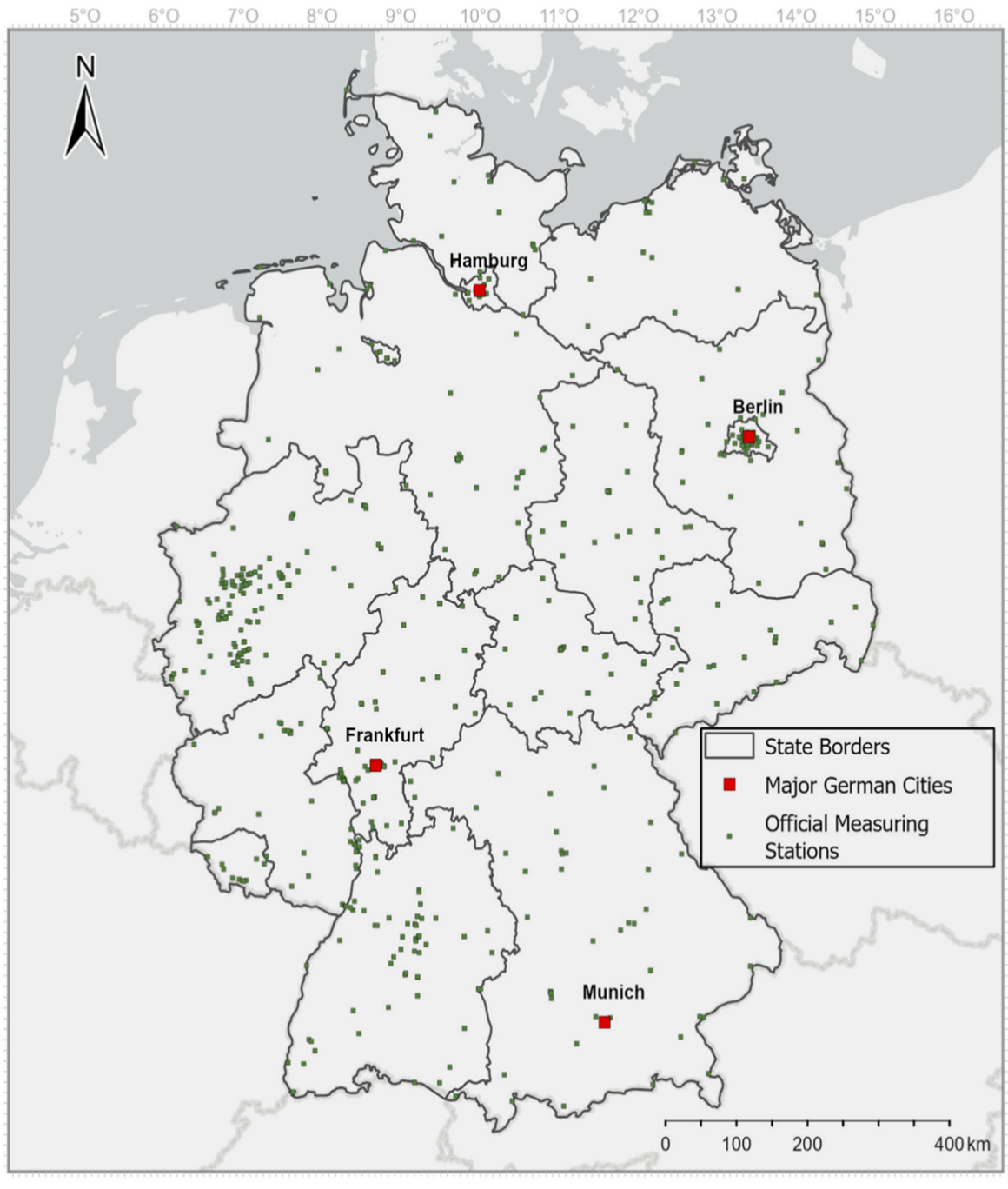

Fig. 1. Map of Germany showing the distribution of major cities (red squares) and the locations of air-quality monitoring stations (green points) from the European air-quality monitoring network (EuroAirnet). (For interpretation of the references to colour in this figure legend, the reader is referred to the Web version of this article.)

European Environment Agency (EEA) air-quality portal, using the European air-quality monitoring network (EuroAirnet) (Larssen et al., 1999). The dataset provides verified measurements of NO_2 and $PM_{2.5}$, reported in μg m^{-3} in accordance with the standards established by Directive (2008)/50/EC. The time period considered spans 2019–2024, with values provided as mean annual concentrations derived from hourly observations compiled in the annual Air Quality Status Reports (European Environment Agency, 2025).

EuroAirnet comprises more than 3500 monitoring stations distributed across all 27 European Union Member States, as well as non-EU countries including Iceland, Liechtenstein, Norway, Switzerland, Türkiye, and several Western Balkan states. For the purposes of this study, only stations located within Germany were selected: approximately 600 stations for NO_2 and 200 stations for $PM_{2.5}$, with slight inter-annual variability in station availability.

Each station record includes geographic coordinates and annual pollutant averages (μg m^{-3}). These coordinates were subsequently used to extract corresponding satellite-derived and meteorological parameters at each monitoring location, enabling the integration of in situ observations with remote-sensing and reanalysis data for model development.

2.2.2. *Remote sensing and climatic reanalysis variables*

The environmental covariates used in this study were retrieved

through the Google Earth Engine (GEE) Python API in Google Colab. These variables represent three main sources of information: atmospheric trace gases measured by Sentinel-5P, vegetation and aerosol indicators derived from MODIS, and near-surface meteorological conditions obtained from the ERA5-Land reanalysis.

For the NO_2 model, the tropospheric NO_2 column from Sentinel-5P served as the primary satellite predictor because it represents the most direct remotely sensed signal associated with surface NO_2; boundary-layer processes often link column abundances with ground-level concentrations (Shetty, 2024). To capture land-surface influences, MODIS Normalized Difference Vegetation Index (NDVI) was incorporated, which reflects vegetation density and structure—factors known to reduce gaseous pollutants through enhanced dry deposition and altered local airflow (Diener and Mudu, 2021). Temperature at 2 m from ERA5-Land was also included, as it influences boundary-layer height and photochemical reaction rates that regulate seasonal NO_2 variability (Guo et al., 2017). Surface pressure from ERA5-Land was used to represent the presence of stagnant, high-pressure conditions that often lead to pollutant build-up near the surface (Boluwade and Ruheili, 2022).

For the $PM_{2.5}$ model, the set of predictors was expanded to represent both primary particle emissions and secondary aerosol processes. Alongside NO_2, we included the tropospheric CO column from Sentinel-5P to capture additional combustion-related activities such as biomass burning and winter heating (Zheng et al., 2023). MODIS NDVI was retained to reflect the role of vegetation in removing particles from the atmosphere (Janhäll, 2015). Meteorological influences were again represented through ERA5-Land temperature and surface pressure, given their importance in secondary aerosol formation and atmospheric mixing (Guo et al., 2017; Boluwade and Ruheili, 2022). To better represent particle abundance, we also incorporated MODIS-MAIAC aerosol optical depth (AOD) at 0.47 μm and 0.55 μm, which remains one of the most widely used satellite-based indicators of surface $PM_{2.5}$ due to its strong correlation with column-integrated light extinction (Handschuh et al., 2023; Schneider, 2020).

All datasets were aggregated to annual medians for the period 2019–2024 to match the temporal resolution of the monitoring-station data. The median was selected instead of the mean because air-pollution distributions are often skewed and influenced by episodic peaks (e.g., winter stagnation events or short-term emission spikes). Using the median reduces the impact of extreme values and provides a more robust estimate of typical annual exposure. For each monitoring location, the corresponding values from all remote-sensing and meteorological collections were extracted, resulting in an integrated dataset linking ground observations with atmospheric and land-surface predictors. The retrieval characteristics and native spatial resolutions of the input datasets are summarised in Table 1.

2.2.3. Machine learning regression and variable importance

Models were trained using a pooled dataset combining observations from all years (2019–2024), rather than fitting separate models for individual years. Calendar year was included as a predictor, allowing the models to capture interannual variability while maximising sample size and stabilising predictor–response relationships. All analyses were conducted in Python using scikit-learn (Pedregosa et al., 2011) within the Google Colab environment. For each year, approximately 3300 NO_2 and 1566 p.m.$_{2.5}$ observations were available from EuroAirnet stations with complete satellite and meteorological covariates extracted via Google Earth Engine. Modelled concentrations were evaluated by extracting predictions at the exact coordinates of monitoring stations to ensure direct comparability with observations.

Seven machine-learning algorithms commonly used in air-quality studies were assessed. Ensemble tree-based models—Random Forest (Breiman, 2001; Yenkikar et al., 2025) and Gradient Boosting (Zhang et al., 2021)—were included due to their ability to capture nonlinear relationships and their strong performance in studies combining TROPOMI, MODIS, and reanalysis data (Long et al., 2022; Mamić et al., 2023). Support Vector Regression was selected for its effectiveness in moderately complex or noisy settings (Özüpak et al., 2025), while k-Nearest Neighbours served as a simple baseline frequently applied in satellite-based $PM_{2.5}$ estimation (Ayinde et al., 2024). Regularised linear models (Ridge, Lasso, and ElasticNet) were used as transparent benchmarks to assess the explanatory power of additive linear relationships while controlling overfitting (Chunyang et al., 2025; Vedrí et al., 2025).

Model performance was first assessed using a 70/30 random train–test split, consistent with previous national-scale studies and suitable for operational mapping. Although spatial cross-validation is often recommended, it can substantially reduce performance estimates when stations are unevenly distributed (Chen et al., 2024). To explicitly assess spatial generalisation, Spatial Block Cross-Validation was applied to the best-performing models, grouping stations into 0.25° (~25–28 km) blocks and withholding entire regions during validation. This design ensures spatial independence between training and validation data and provides a conservative assessment of performance in poorly monitored areas (Bagkis et al., 2025). Hyperparameters optimised under random cross-validation were reused for Spatial CV to ensure comparability.

Hyperparameter tuning was performed using RandomizedSearchCV, enabling efficient exploration of influential parameter combinations (Karthick et al., 2024). Optimisation targeted model-specific parameters for each algorithm and was conducted separately for NO_2 and $PM_{2.5}$. Performance was evaluated using RMSE and R^2 for both validation strategies, capturing prediction error magnitude and explained variance

Table 1
Overview of the remote-sensing and climate reanalysis parameters used in this study, retrieved through GEE. The table summarizes each dataset's source, variable type, and spatial characteristics.

Parameter	GEE Catalogue	Equation or Algorithm	Spatial Resolution (m)	Column name in the datasets
Sentinel-5P OFFL NO2: Offline Nitrogen Dioxide	COPERNICUS/S5P/OFFL/L3_NO2 Band: tropospheric_NO2_column_number_density	Sentinel-5P OFFL NO_2 processor (DOAS + AMF) (van Geffen et al., 2022; Lange et al., 2023)	1113	NO2_median
MOD13Q1.061 Terra Vegetation Indices 16-Day Global 250m	MODIS/061/MOD13Q1 Band: NDVI	*(Near Infrared-Red)/(Near Infrarred + Red)* Huete et al. (2002)	250	NDVI_median
ERA5-Land Daily Aggregated - ECMWF Climate Reanalysis	ECMWF/ERA5_LAND/DAILY_AGGR Bands: temperature_2m surface_pressure	4D-Var data-assimilation replay (Hersbach et al., 2020; Muñoz-Sabater et al., 2021)	11,132	T2M_median_C SP_median_hPa
Sentinel-5P OFFL CO: Offline Carbon Monoxide	COPERNICUS/S5P/OFFL/L3_CO Band: CO_column_number_density	Sentinel-5P OFFL CO optimal-estimation retrieval (Borsdorff et al., 2018)	1113	CO_median
MCD19A2.061: Terra & Aqua MAIAC Land Aerosol Optical Depth Daily 1 km	MODIS/061/MCD19A2_GRANULES Bands: Optical_Depth_047 Optical_Depth_055	MAIAC aerosol optical depth (AOD) inversion Lyapustin & Wang (2018)	1000	AOD_047_median AOD_055_median

(Venter et al., 2020; Muthukumar et al., 2022).

To assess interpretability and physical consistency, the best-performing model for each pollutant was analysed using SHAP values, which quantify the contribution of individual predictors to model outputs (Houdou et al., 2024). SHAP is a game-theory-based approach that decomposes individual model predictions into additive contributions from each predictor variable, based on Shapley values originally developed in cooperative game theory. This method provides both global and local interpretability: globally, it ranks variables according to their overall influence on model outputs; locally, it quantifies how specific predictor values increase or decrease individual predictions. In this study, SHAP summary plots were generated to examine the magnitude and direction of variable contributions across monitoring sites. SHAP has become increasingly relevant in air-quality research for evaluating whether learned relationships align with known atmospheric processes and for identifying key drivers of pollutant variability (Hou et al., 2025), particularly in applications supporting monitoring networks or policy-relevant exposure assessments.

2.2.4. Sensitivity analysis: Inclusion of road density (static variables)

To complement the main modelling framework based solely on dynamic, annually varying predictors, an additional sensitivity analysis was performed to examine the potential contribution of a static road-density indicator. Road transport remains one of the most important sources of NO_x emissions in Germany, accounting for nearly 60% of national transport-related NO_x in recent years (UBA, 2024). As a result, traffic-related indicators are frequently used to capture local emission gradients and remain among the strongest spatial predictors of surface NO_2 in many European studies (Essamlali et al., 2025).

To reflect this well-established relationship, a high-resolution road-density layer was derived using the Global Roads Inventory Project (GRIP) dataset (Meijer et al., 2018), following the processing approach outlined in Balamurugan et al. (2023). The GRIP shapefile was clipped to the German boundary, and a regular grid of 1 km × 1 km was generated across the country. For each grid cell, we calculated the total length of roads, producing a continuous road-density raster from which values were extracted at each EuroAirnet station location.

Because road density does not change from year to year, it does not capture inter-annual shifts in emissions, meteorology, or atmospheric chemistry. For this reason, and in line with our objective to evaluate predictors that vary annually, road density was not included in the core modelling framework. Instead, it was incorporated only in a dedicated set of sensitivity experiments to assess how much additional spatial information this static traffic proxy provides (Wang et al., 2021).

These tests used the same modelling configurations as the main analysis, including identical random and spatial cross-validation settings and the same hyperparameter optimisation strategy—so that any performance gain could be attributed solely to the presence of the road-density variable.

Fig. 2 summarizes the complete modelling workflow.

3. Results

3.1. Air monitoring network data analysis in Germany

A first inspection of the EuroAirnet dataset shows 3300 annual mean NO_2 observations between 2019 and 2024, revealing a clear nationwide decline with marked spatial and temporal variability (Fig. S1). Concentrations were highest in 2019 and lowest in 2024, with the strongest reductions occurring between 2019 and 2021, coinciding with COVID-19–related mobility restrictions. A partial rebound is evident in 2022, followed by continued declines thereafter. Annual means remained below the former EU limit of 40 μg m^{-3} throughout the period, although most stations consistently exceeded the WHO guideline of 10 μg m^{-3}. The narrowing distribution over time indicates a reduction in high-concentration hotspots, reflected in the sharp decrease in stations exceeding the EU limit from 2019 onward. These patterns indicate substantial improvements in NO_2 air quality, while highlighting the challenge of meeting health-based thresholds and forthcoming stricter EU standards.

A total of 1556 annual $PM_{2.5}$ observations were available for the same period, showing a more gradual and heterogeneous evolution than

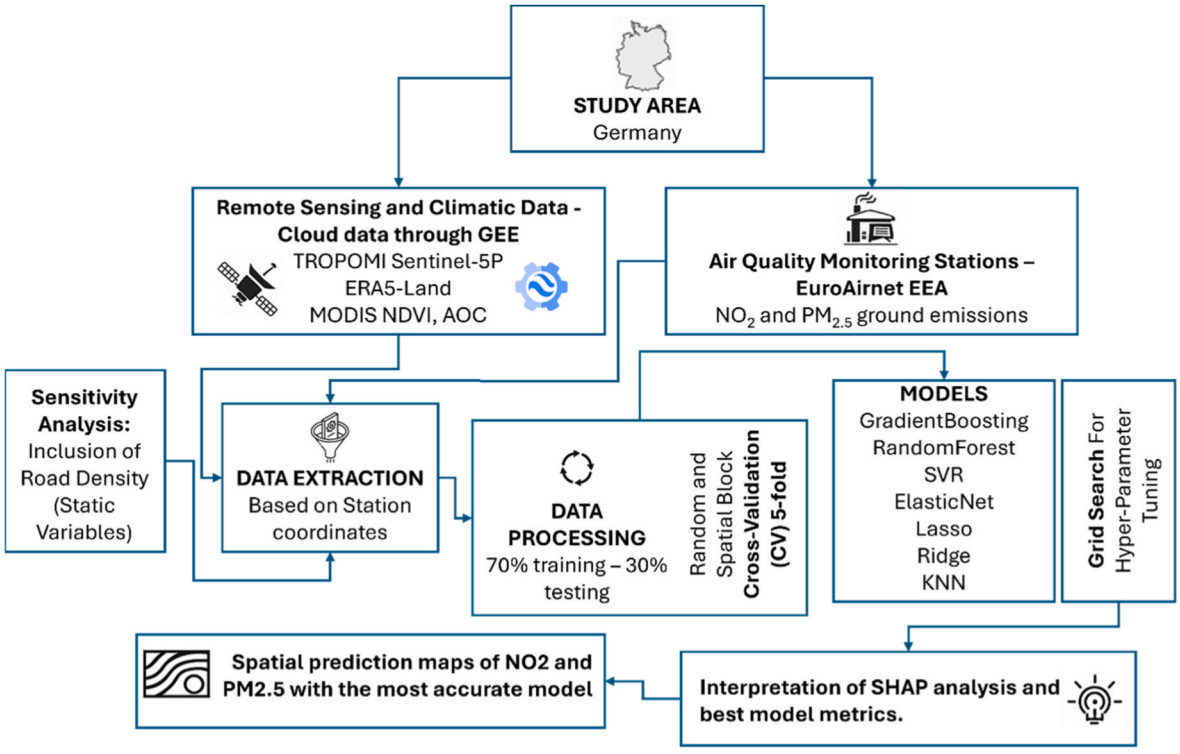

Fig. 2. Workflow diagram of the study.

NO_2 (Fig. S2). Concentrations decreased in 2020, rebounded in 2021, and exhibited further year-to-year variability thereafter, although mean and median values suggest a modest long-term decline. $PM_{2.5}$ displays smaller interannual variability and more compact distributions, consistent with its regional character and influence from secondary formation and long-range transport. Annual means remained below the EU limit of 25 μg m^{-3} but exceeded the WHO guideline of 5 μg m^{-3} at most stations each year. These results point to incremental improvements in $PM_{2.5}$ air quality, while persistent exceedances of health-based guidelines underscore the need for sustained emission reductions under the new regulatory framework.

3.2. Correlation analysis between explanatory variables

Figs. S3 and S4 show the Pearson correlation coefficients for the variables used to model annual mean NO_2 and $PM_{2.5}$ concentrations. The correlations are mostly weak to moderate, as expected for a national dataset spanning different climatic regions, land-cover types, and emission environments.

For NO_2 (Fig. S3), the annual mean concentrations display only weak correlations with most meteorological and geographic variables. The correlation with year is slightly negative (−0.26), indicating a gradual reduction in NO_2 levels over the study period. Temperature and surface pressure also show weak relationships with NO_2, while latitude and longitude have little influence on the annual means. More noticeable is the moderate positive correlation between ground-measured NO_2 and the satellite-derived NO_2 column ($r = 0.53$), indicating a clear statistical link between the two datasets. NDVI shows a moderate negative correlation with NO_2 ($r = -0.62$), and the satellite NO_2 column also correlates moderately with longitude (−0.54). These patterns simply describe how the underlying datasets vary relative to one another across the measurement locations.

The correlation results for $PM_{2.5}$ (Fig. S4) reveal a similar structure. $PM_{2.5}$ shows a weak-to-moderate negative correlation with year (−0.39), indicating a downward trend over the six-year period. NDVI again presents a moderate negative correlation (−0.46). Moderate positive correlations are observed between $PM_{2.5}$ and satellite-derived NO_2 ($r = 0.40$), as well as with surface pressure (0.35). By contrast, temperature shows only a very weak relationship with $PM_{2.5}$, and the two MAIAC AOD products at 470 nm and 550 nm exhibit negligible correlations with the ground-based $PM_{2.5}$ values. Both AOD bands show only very small correlations with year.

Taken together, these results indicate that no pair of variables is strongly collinear, and that several predictors—such as NDVI, satellite-derived NO_2, and surface pressure-exhibit clearer statistical associations with the pollutant concentrations than others.

3.3. Air concentration modelling

The machine-learning experiments produced distinct performance patterns across algorithms and pollutants. For NO_2, ensemble tree-based models achieved the best results (Table S1). Random Forest reached a cross-validated RMSE of 6.13 μg m^{-3} (CV $R^2 = 0.65$) and a test RMSE of 5.87 μg m^{-3} (test $R^2 = 0.68$). Gradient Boosting performed similarly, with a CV RMSE of 6.32 μg m^{-3} (CV $R^2 = 0.62$) and a test RMSE of 6.13 μg m^{-3} (test $R^2 = 0.65$).

Models such as SVR, Ridge, Lasso, ElasticNet and KNN produced higher errors and substantially lower R^2 values. Under Spatial Block Cross-Validation, NO_2 performance decreased for all algorithms, reflecting the more stringent geographic separation between training and testing regions. Random Forest achieved a Spatial CV RMSE of 7.15 μg m^{-3} (Spatial CV $R^2 = 0.50$), and Gradient Boosting achieved 7.04 μg m^{-3} (Spatial CV $R^2 = 0.51$). The remaining algorithms showed lower spatial R^2 values, ranging from 0.03 to 0.35. The predicted-versus-observed NO_2 plot (Fig. S5) shows a clear positive association between measured and predicted values, with closer agreement at moderate concentrations and wider dispersion at higher values.

The SHAP summary plot for NO_2 (Fig. 3) shows that Sentinel-5P NO_2 and NDVI contribute the largest variation in SHAP values, followed by meteorological predictors. The distribution of SHAP points reflects the relative contribution magnitudes and the range of predictor values across sites.

For $PM_{2.5}$, Gradient Boosting achieved the strongest results (Table S2), with a CV RMSE of 11.61 μg m^{-3} (CV $R^2 = 0.56$) and a test RMSE of 11.53 μg m^{-3} (test $R^2 = 0.50$). Random Forest showed similar but slightly weaker performance. The linear models, SVR and KNN produced higher RMSE and lower R^2 values. Under Spatial CV, $PM_{2.5}$ performance decreased for all models. Gradient Boosting produced a Spatial CV RMSE of 13.33 μg m^{-3} (Spatial CV $R^2 = 0.36$), while Random Forest achieved 13.37 μg m^{-3} (Spatial CV $R^2 = 0.36$). The remaining models produced Spatial CV R^2 values between 0.07 and 0.26.

The $PM_{2.5}$ observed-versus-predicted plot (Fig. S6) shows a positive trend and a wider scatter than the NO_2 plot, indicating higher uncertainty across the $PM_{2.5}$ modelling framework.

The SHAP summary plot for $PM_{2.5}$ (Fig. 4) shows the ranked influence of each predictor in the Gradient Boosting model. Surface pressure exhibits the greatest spread of SHAP values, followed by NDVI, Sentinel-5P NO_2, CO, and temperature. The two AOD variables (AOD_055 and AOD_047) exhibit narrow SHAP distributions centred near zero, indicating limited contribution under the annual modelling configuration. The colour gradients reflect the range of predictor values across monitoring stations, while the horizontal spread of points represents the magnitude of the variable-specific contributions to individual predictions.

3.4. Sensitivity analysis (static road-density variable)

A separate sensitivity analysis evaluated the effect of including a static 1-km road-density layer (Table 2). This variable was included solely for this test and was not retained in the final modelling configuration.

For NO_2, including road density, improved several performance metrics. Gradient Boosting showed a reduction in CV RMSE from 6.32 to 5.54 μg m^{-3} and an increase in CV R^2 from 0.62 to 0.68. Test R^2 increased from 0.65 to 0.71.

Under Spatial CV, Gradient Boosting reached a Spatial CV RMSE of 6.92 μg m^{-3} (Spatial CV $R^2 = 0.47$). Random Forest showed similar patterns, with CV RMSE decreasing from 6.13 to 5.93 μg m^{-3} and Spatial CV R^2 changing from 0.50 to 0.46.

For $PM_{2.5}$, improvements were smaller. Test R^2 increased slightly from 0.50 to 0.55 for Gradient Boosting, while Spatial CV R^2 remained similar (≈0.27). SHAP values indicate that, unlike NO_2, $PM_{2.5}$ is dominated by meteorological variables and secondary aerosol processes, and the static road-density proxy contributes less information at the annual scale.

Because road density enhanced results only in specific station-dense urban regions—and not at the national-scale generalisation level—the variable was excluded from the final modelling configuration.

3.5. National air concentration (NO_2 and $PM_{2.5}$) maps for Germany (2019–2024)

National maps of annual NO_2 and $PM_{2.5}$ concentrations across Germany (2019–2024) were generated using the final Random Forest and Gradient Boosting models on a 10-km grid based on annual medians, respectively. The NO_2 surfaces show a consistent nationwide decline (Fig. 5), with the strongest reductions observed in major urban and industrial regions, in agreement with monitoring-station measurements. In contrast, $PM_{2.5}$ exhibits weaker spatial gradients and more heterogeneous temporal behaviour, including a temporary increase in 2022 followed by lower levels in 2024, reflecting both mixed formation processes and the moderate predictive performance of the model (Fig. 6).

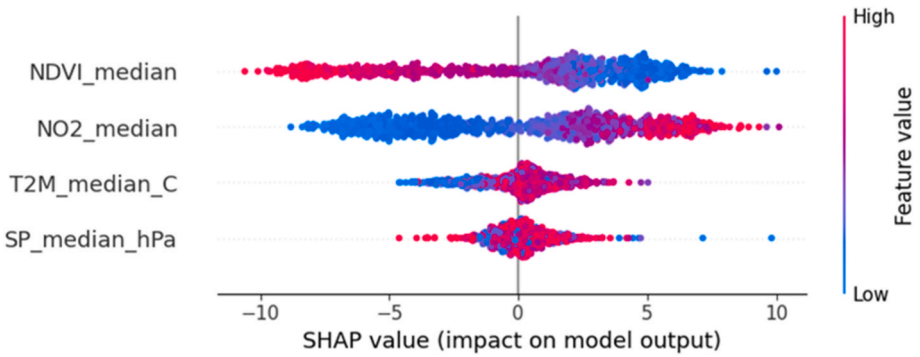

Fig. 3. SHAP summary plot for NO_2 predictions (2019–2024). The x-axis shows SHAP values (feature impact on the model), and the y-axis lists the ranked predictor variables.

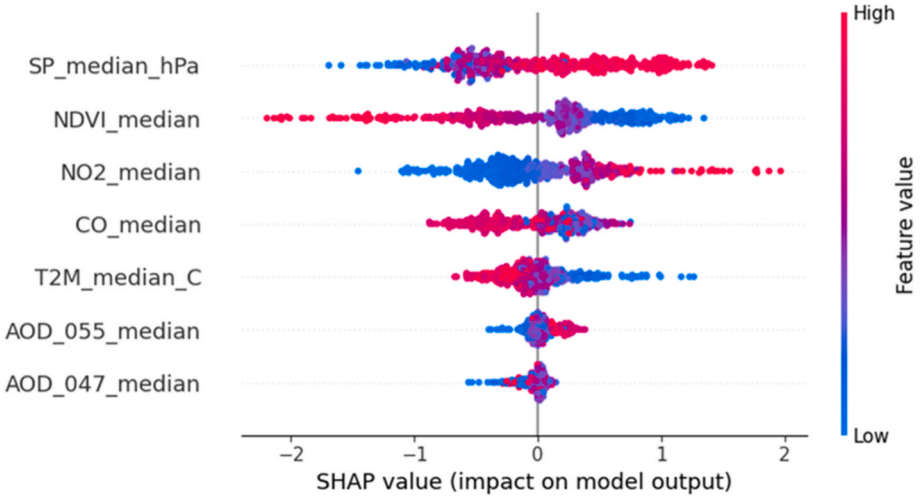

Fig. 4. SHAP summary plot for $PM_{2.5}$ predictions (2019–2024). The x-axis shows SHAP values (feature impact on the model), and the y-axis lists the ranked predictor variables.

Table 2
Performance metrics for the sensitivity experiment, including the static 1-km road-density variable.

Pollutant	Model	CV RMSE	CV R^2	Test RMSE	Test R^2	Spatial CV RMSE	Spatial CV R^2
NO_2	GradientBoosting	5.539	0.682	5.329	0.706	6.917	0.466
	RandomForest	5.928	0.635	5.961	0.633	6.966	0.459
$PM_{2.5}$	GradientBoosting	1.092	0.572	1.051	0.550	1.429	0.275
	RandomForest	1.131	0.541	1.092	0.514	1.442	0.264

Overall, the maps provide a spatially explicit overview of recent air-quality changes and support the integration of satellite observations, meteorological reanalysis, and machine-learning methods for national-scale assessments.

To complement the spatial prediction maps, the agreement between modelled and observed concentrations at monitoring locations is illustrated in Figs. S5 and S6 (Supplementary Material). These scatter plots provide a direct comparison between predicted and measured annual values and demonstrate that the model reproduces the main concentration gradients observed in the monitoring network. Given the 10 km modelling resolution, the concentration surfaces represent background spatial patterns rather than site-specific micro-scale variability.

4. Discussion

This study shows that freely available satellite observations, ERA5-Land meteorology, and machine-learning models can be combined to characterise annual NO_2 and $PM_{2.5}$ patterns across Germany between 2019 and 2024. Because the framework relies exclusively on open datasets, it is particularly relevant for regions with sparse or uneven monitoring coverage. The results also highlight clear differences between gaseous and particulate pollutants, illustrating the strengths and limitations of annual satellite-derived predictors in national-scale air-quality assessments.

For NO_2, both observations and model outputs indicate a steady decline over the study period, consistent with reduced road-traffic emissions, fleet improvements, and pandemic-related mobility changes, in line with previous European assessments (Petetin et al., 2020; Grange et al., 2021). Among the evaluated algorithms, Random Forest performed best. SHAP analysis confirmed the dominant role of physically meaningful predictors, particularly Sentinel-5P tropospheric NO_2 columns, which have been shown to relate well to surface concentrations across Europe (Chan et al., 2021; Virta et al., 2023), and NDVI, which differentiates vegetated from transport-dominated environments influencing dispersion and deposition (Shetty, 2024). These findings suggest that annual NO_2 variability can be reasonably captured

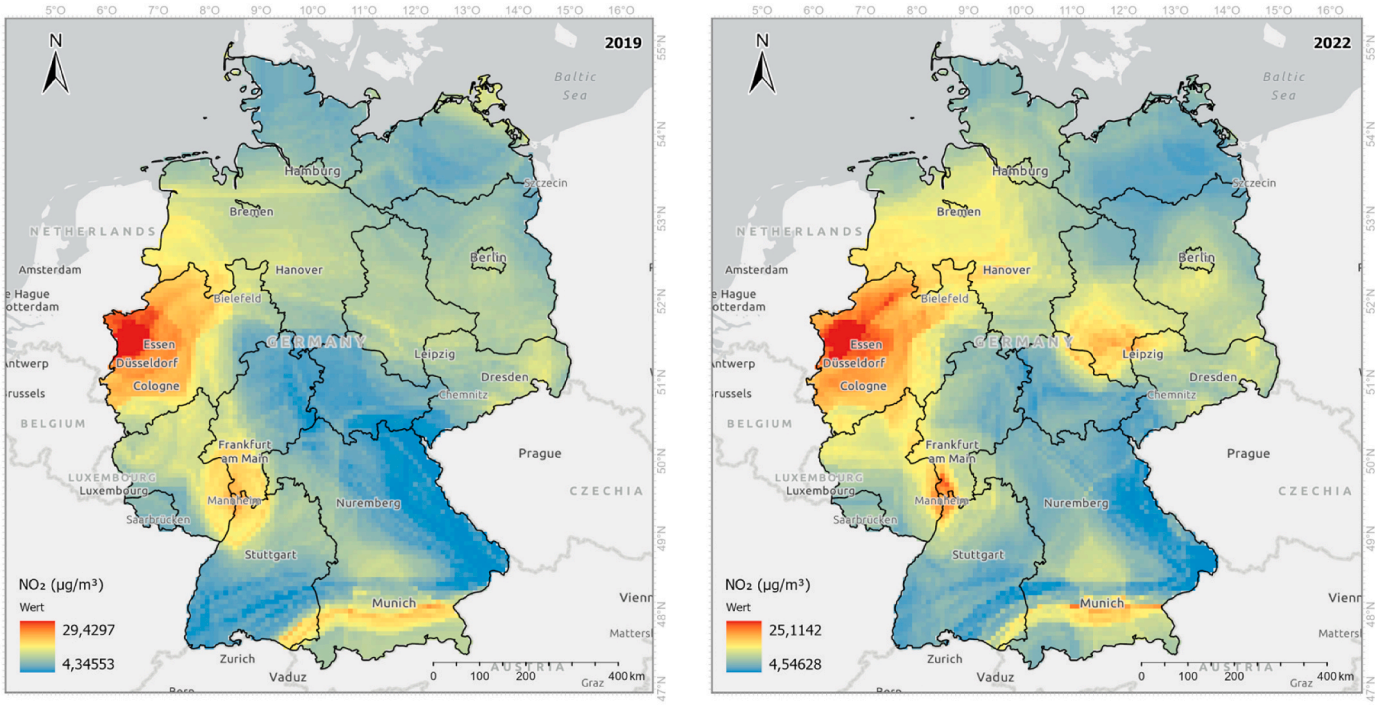

(a)

(b)

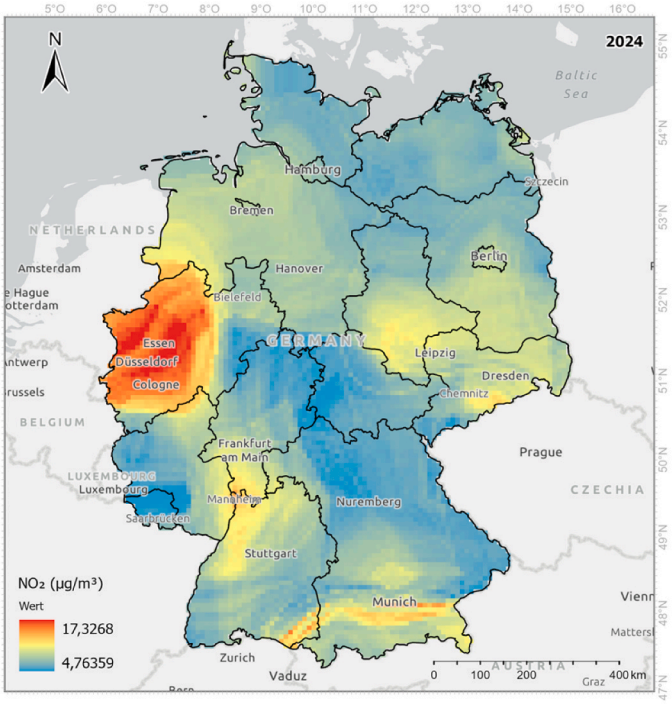

(c)

Fig. 5. Predicted national NO_2 concentrations for Germany in (a) 2019, (b) 2022 and (c) 2024 generated using the best-performing model (10 km grid).

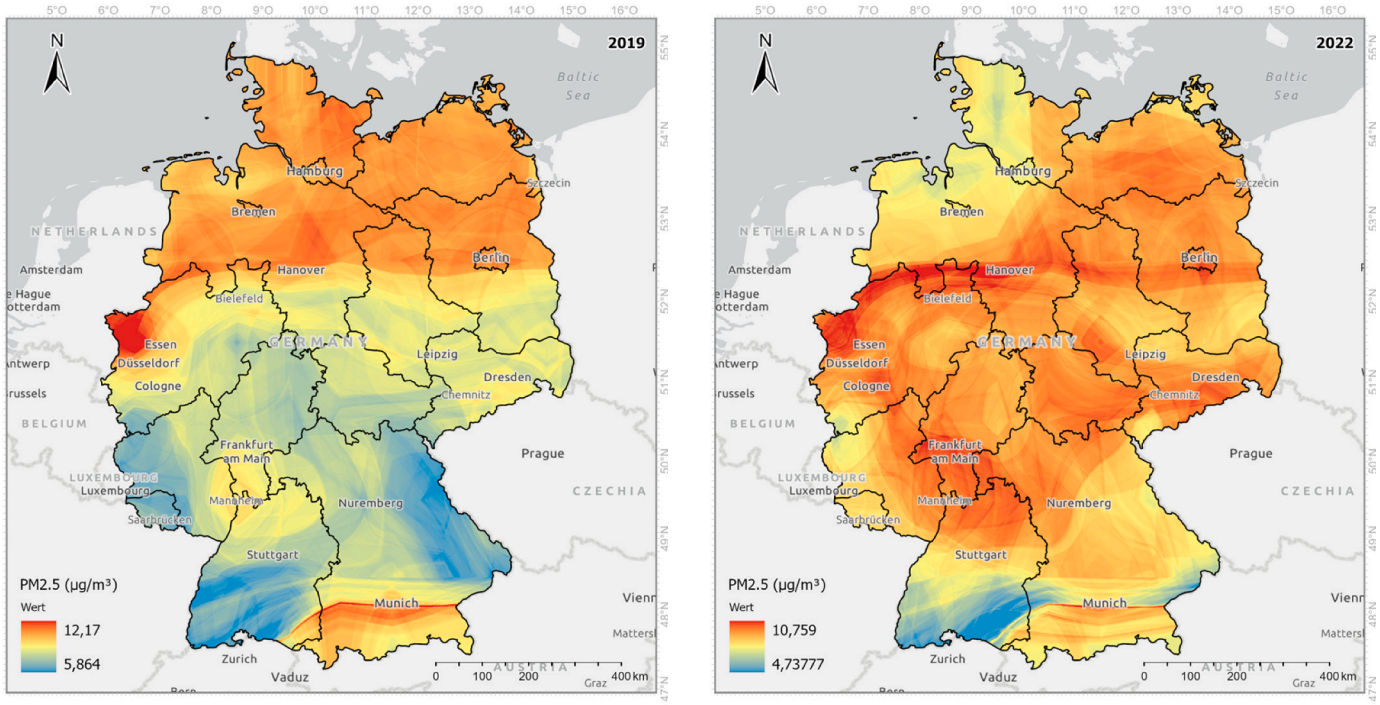

(a) (b)

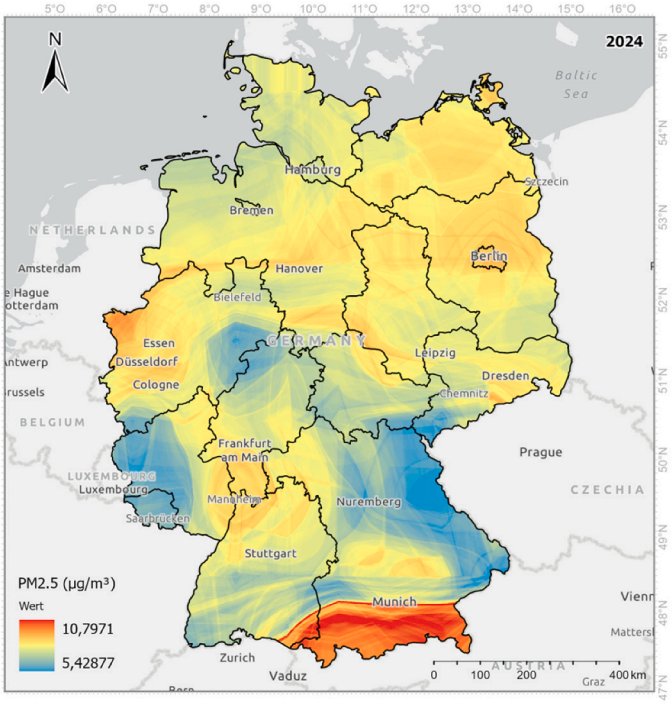

(c)

Fig. 6. Predicted national $PM_{2.5}$ concentrations for Germany in (a) 2019, (b) 2022 and (c) 2024 generated using the best-performing model (10 km grid).

using dynamic satellite- and reanalysis-based inputs.

Despite this performance (RMSE ≈ 6 μg m^{-3}), the modelling framework is not intended for regulatory compliance or enforcement purposes. Annual limit values are defined at individual monitoring locations and require uncertainty levels that cannot be achieved with a coarse, national-scale satellite-driven approach. Instead, the model is designed to represent large-scale spatial gradients, long-term tendencies, and contrasts between emission environments, providing an area-averaged background concentration field that complements, rather than replaces, in-situ monitoring.

$PM_{2.5}$ exhibited more complex behaviour. Although a long-term decline is evident, interannual variability was larger than for NO_2, reflecting the influence of winter heating, secondary aerosol formation, and meteorological stagnation, as widely reported for Germany and central Europe (Pietikäinen et al., 2015; Liu et al., 2021). Gradient Boosting achieved the best performance for $PM_{2.5}$, albeit with moderate accuracy, consistent with the diverse sources and processes controlling particulate matter, including precursor gases, long-range transport, humidity, and boundary-layer dynamics (Bae et al., 2020). SHAP analysis identified surface pressure, NDVI, and NO_2 as the most influential predictors, while MAIAC AOD contributed little at the annual scale, in agreement with previous studies showing weakened AOD–$PM_{2.5}$ relationships under long-term aggregation (Zheng et al., 2017; Damascena et al., 2021). Consequently, the $PM_{2.5}$ maps should be interpreted as broad regional gradients rather than fine-scale local estimates.

Model evaluation strategy influenced performance interpretation. Random cross-validation was used as the primary approach, as strict spatial blocking can produce unstable or overly conservative estimates when monitoring stations are unevenly distributed (Wadoux et al., 2021; Ochege et al., 2025). Given the objective of developing reproducible national-scale models comparable to data-limited regions, random cross-validation provided a practical compromise, although some spatial dependence likely remains. The relevance of traffic-related processes is nevertheless supported by the strong contribution of Sentinel-5P NO_2 and by sensitivity tests using a static road-density proxy.

The sensitivity analysis showed that road density improved NO_2 performance under random cross-validation, with weaker gains under spatial validation, suggesting benefits for local fitting rather than national generalisation, consistent with earlier findings (Balamurugan et al., 2021, 2023). Effects for $PM_{2.5}$ were modest, reflecting the dominance of regional and meteorological drivers. Road density was therefore excluded from the final models to maintain a focus on dynamic predictors, although its relevance for urban-scale applications is evident.

The core modelling framework intentionally prioritises dynamic predictors that vary annually (satellite-derived atmospheric variables and meteorological reanalysis), rather than static land-use layers. This design choice enhances temporal consistency, reproducibility, and transferability across regions where detailed land-use inventories may not be available. The sensitivity analysis including road density confirms that static variables can improve local fitting near monitoring stations, but their contribution to national-scale spatial generalisation remains limited.

The resulting concentration surfaces capture dominant national patterns: a consistent decline in NO_2 across urban and rural areas, and more heterogeneous behaviour for $PM_{2.5}$. SHAP results indicate reliance on predictors consistent with known atmospheric processes, supporting the internal physical coherence of the models (Gu et al., 2021). The smooth appearance of the maps reflects annual aggregation and the 10-km grid resolution, representing background concentration fields rather than intra-urban variability. Persistent features, such as elevated values around Munich, align with stable tropospheric NO_2 and land-use characteristics rather than modelling artefacts.

From a policy perspective, the findings indicate continued improvements in German air quality, while also showing that many locations remain above current WHO guideline values. In the context of Directive (EU) 2024/2881 (European Parliament & Council of the EU, 2024) and its stricter future limits, the presented framework can support national assessments by providing a spatially continuous complement to monitoring networks. Its reliance on globally available open data also facilitates transferability to regions lacking dense observational coverage (Im et al., 2025).

Future work could explore higher-temporal-resolution predictors, additional meteorological and chemical variables (e.g., boundary-layer height, humidity, and precursor gases), and more advanced spatial–temporal validation strategies (Berrisford et al., 2025). Integrating national emission inventories, such as kilometre-scale datasets from the German Environment Agency, may further improve urban-scale performance but was intentionally excluded here to preserve global applicability. Emerging satellite embedding products and deep-learning architectures may also help capture finer-scale variability in future applications (Alvarez et al., 2025).

5. Conclusion

This study shows that open satellite observations, reanalysis data, and machine-learning models can be combined to characterise annual NO_2 and $PM_{2.5}$ concentrations across Germany for the period 2019–2024 using only freely available predictors. The models reproduce the main spatial patterns observed at monitoring stations, with higher predictive performance for NO_2, reflecting its strong association with traffic-related proxies and Sentinel-5P tropospheric NO_2. In contrast, $PM_{2.5}$ exhibits greater complexity, consistent with the influence of multiple sources, secondary aerosol formation, and meteorological processes that are less well captured by annually aggregated inputs.

SHAP analysis indicates that tropospheric NO_2 and vegetation structure are the most influential predictors for NO_2, while surface pressure, NDVI, and co-emitted gases dominate $PM_{2.5}$ predictions, with annual AOD contributing limited additional information. Including road density improves NO_2 performance under random cross-validation but has a weaker effect under spatial validation, suggesting limited transferability at national scale.

The modelled concentration surfaces capture the multi-year decline in NO_2 and the more heterogeneous evolution of $PM_{2.5}$. Although annual models cannot resolve short-term variability, the approach provides a transparent and reproducible framework for national air-quality assessment based entirely on open datasets. Further improvements may be achieved by incorporating higher-temporal-resolution predictors, additional chemical and boundary-layer variables, and hybrid spatial–temporal validation strategies.

CRediT authorship contribution statement

Rebecca Miller: Writing – original draft, Investigation. **Jonas Olbrich:** Writing – original draft, Investigation. **Wierer Manuel:** Writing – original draft, Investigation. **Jia Chen:** Writing – review & editing, Validation. **Michael Wurm:** Writing – review & editing, Visualization, Validation. **Cesar Ivan Alvarez:** Writing – review & editing, Writing – original draft, Supervision, Methodology, Investigation, Conceptualization.

Availability of data and material

All remotely sensed data and ground-based air-quality measurements used in this study are publicly available from their respective providers (Copernicus Sentinel-5P, MODIS, ERA5-Land, and the European Environment Agency).

The Python scripts used for data processing, feature extraction via Google Earth Engine, machine-learning model development, and map generation are available from the corresponding author upon reasonable request.

Declaration of generative AI and AI-assisted technologies in the writing process

During the preparation of this work, the authors used ChatGPT 5.1 and Grammarly to improve English grammar and clarity. After using these tools, the authors reviewed and edited the content as needed and took full responsibility for the final version of the manuscript.

Funding

This research received no specific grant from any funding agency in the public, commercial, or not-for-profit sectors. Jia Chen is supported by the European Research Council (ERC) under the European Union's Horizon Europe research and innovation programme, Consolidator Grant CoSense4Climate (Grant Agreement No. 101089203).

Declaration of competing interest

The authors declare that they have no known competing financial interests or personal relationships that could have appeared to influence the work reported in this paper.

Acknowledgements

We thank the students and lecturer of the Environmental Modelling and Health course (MSc Geoinformatics, University of Augsburg, Germany, Summer Semester 2025/2026) for their support during this study. We also acknowledge the contributions of the co-authors and the Chair of Climate Resilience of Cultural Ecosystems at the Center for Climate Resilience, University of Augsburg, Germany. We are grateful to Vignesh Balamurugan for his constructive comments on the manuscript.

Appendix A. Supplementary data

Supplementary data to this article can be found online at https://doi.org/10.1016/j.envpol.2026.127898.

Data availability

Data will be made available on request.

References

Alvarez, C.I., López, S., Gualotuña, D., 2026. Atmospheric composition and sensing. In: Huang, X., Wang, S., Kalogeropoulos, K., Tsatsaris, A. (Eds.), Data-Driven Earth Observation for Disaster Management. Elsevier, pp. 431–442. https://doi.org/10.1016/B978-0-443-33803-8.00043-3.

Alvarez, C.I., Ulloa Vaca, C.A., Echeverria Llumipanta, N.A., 2025. Machine learning for urban air quality prediction using google AlphaEarth foundations satellite embeddings: a case study of Quito, Ecuador. Remote Sens. 17 (20), 3472. https://doi.org/10.3390/rs17203472.

Alvarez-Mendoza, C.I., Teodoro, A.C., Torres, N., Vivanco, V., 2019. Assessment of remote sensing data to model PM10 estimation in cities with a low number of air quality stations: a case of Study in Quito, Ecuador. Environments 6 (7), 85. https://doi.org/10.3390/environments6070085.

Anggraini, T.S., Irie, H., Sakti, A.D., Wikantika, K., 2024. Machine learning-based global air quality index development using remote sensing and ground-based stations. Environ. Adv. 15, 100456. https://doi.org/10.1016/j.envadv.2023.100456.

Anggraini, T.S., Irie, H., Sakti, A.D., Wikantika, K., 2025. Global air quality index prediction using integrated spatial observation data and geographics machine learning. Science of Remote Sensing 11, 100197. https://doi.org/10.1016/j.srs.2025.100197.

Ayinde, B.O., Musa, M.R., Ayinde, A.O., 2024. Application of machine learning models and Landsat-8 data for estimating seasonal PM2.5 concentrations. Environmental Analysis Health and Toxicology 39 (1). https://doi.org/10.5620/eaht.2024011 e2024011-0.

Bae, C., Kim, B.-U., Kim, H.C., Yoo, C., Kim, S., 2020. Long-Range transport influence on key chemical components of PM2.5 in the Seoul metropolitan area. Atmosphere 11 (1), 48. https://doi.org/10.3390/atmos11010048.

Bagkis, E., Hassani, A., Schneider, P., et al., 2025. Evolving trends in application of low-cost air quality sensor networks: challenges and future directions. npj Clim. Atmos. Sci. 8, 335. https://doi.org/10.1038/s41612-025-01216-4.

Balamurugan, V., Chen, J., Qu, Z., Bi, X., Gensheimer, J., Shekhar, A., et al., 2021. Tropospheric NO_2 and O_3 response to COVID-19 lockdown restrictions in Germany. J. Geophys. Res. Atmos. 126. https://doi.org/10.1029/2021JD035440 e2021JD035440.

Balamurugan, V., Chen, J., Wenzel, A., Keutsch, F.N., 2023. Spatiotemporal modeling of air pollutant concentrations in Germany using machine learning. Atmos. Chem. Phys. 23, 10267–10285. https://doi.org/10.5194/acp-23-10267-2023.

Berrisford, L.J., Barbosa, H., Menezes, R., 2025. A data-driven supervised ML approach to estimating global ambient air pollution with prediction intervals. R. Soc. Open Sci. 12, 241288. https://doi.org/10.1098/rsos.241288.

Boluwade, A.M., Ruheili, A., 2022. Modeling NO_2, vertical pressure velocity and PM2.5 contributions to COVID-19 fatalities. Stoch. Environ. Res. Risk Assess. 36, 3487–3498. https://doi.org/10.1007/s00477-022-02205-2.

Borsdorff, T., et al., 2018. Sentinel-5P TROPOMI carbon monoxide retrieval algorithm. Atmos. Meas. Tech. 11, 2135–2148. https://doi.org/10.5194/amt-11-2135-2018.

Breiman, L., 2001. Random forests. Mach. Learn. 45, 5–32. https://doi.org/10.1023/A:1010933404324.

Chan, K.L., Khorsandi, E., Liu, S., Baier, F., Valks, P., 2021. Estimating surface NO_2 over Germany using TROPOMI and ML. Remote Sens. 13 (5), 969. https://doi.org/10.3390/rs13050969.

Chauhan, R., Kaur, H., Alankar, B., 2021. Air quality forecast using convolutional neural network for sustainable development in urban environments. Sustain. Cities Soc. 75, 103239. https://doi.org/10.1016/j.scs.2021.103239.

Chen, Q., Shao, K., Zhang, S., 2024. Enhanced PM2.5 estimation across China: an AOD-independent two-stage approach incorporating improved spatiotemporal heterogeneity representations. J. Environ. Manag. 368, 122107. https://doi.org/10.1016/j.jenvman.2024.122107.

Chunyang, Zhao, Zhang, S., Zhang, B., Tian, H., Yan, G., Zhao, H., 2025. Identification of B-cell biomarkers in endometriosis. Am. J. Reprod. Immunol. 94 (3). https://doi.org/10.1111/aji.70159.

Damascena, A.S., et al., 2021. Relationship between high-resolution AOD and PM in São Paulo. Atmos. Environ. 244, 117949. https://doi.org/10.1016/j.atmosenv.2020.117949.

Diener, A., Mudu, P., 2021. How vegetation protects from air pollution. Sci. Total Environ. 796, 148605. https://doi.org/10.1016/j.scitotenv.2021.148605.

Didan, K., 2021. MODIS/Terra vegetation indices (MOD13A2 V061). NASA LP DAAC. https://doi.org/10.5067/MODIS/MOD13A2.061.

EEA, 2023. Air quality in Europe — 2023 report. https://www.eea.europa.eu/en/analysis/publications/europes-air-quality-status-2023.

EEA, 2024. Harm to human health from air pollution in Europe: burden of disease 2024. https://www.eea.europa.eu/en/analysis/publications/harm-to-human-health-from-air-pollution-2024.

EEA, 2025. Air quality download service. https://www.eea.europa.eu/en/datahub/datahubitem-view/778ef9f5-6293-4846-badd-56a29c70880d.

Essamlali, I., Nhaila, H., Khaili, M.E., 2025. Urban block shape impacts on traffic and air quality. Transp. Res. Interdiscip. Perspect. 31, 101413. https://doi.org/10.1016/j.trip.2025.101413.

European Parliament & Council of the EU, 2008. Directive 2008/50/EC on Ambient Air Quality.

European Parliament & Council of the EU, 2024. Directive (EU) 2024/2881 on Ambient Air Quality (recast).

European Space Agency, 2018. Copernicus Sentinel-5P TROPOMI NO_2 L2 products. https://doi.org/10.5270/S5P-s4ljg54.

Grange, S.K., et al., 2021. COVID-19 lockdowns and ozone increase in European cities. Atmos. Chem. Phys. 21, 4169–4185. https://doi.org/10.5194/acp-21-4169-2021.

Gu, J., Yang, B., Brauer, M., Zhang, K.M., 2021. Improving interpretability of data-driven air quality models. Atmos. Environ. 246, 118125. https://doi.org/10.1016/j.atmosenv.2020.118125.

Guo, J., et al., 2017. Influence of diurnal cycles and meteorology on PM2.5–AOD. Environ. Pollut. 221, 104. https://doi.org/10.1016/j.envpol.2016.11.043.

Hahad, O., Lelieveld, J., Al-Kindi, S., et al., 2025. Burden of disease in Germany from PM pollution. Herz 50, 42–50. https://doi.org/10.1007/s00059-024-05269-8.

Handschuh, J., Erbertseder, T., Baier, F., 2023. Evaluation of satellite AOD datasets for PM2.5 via Random forest. Remote Sens. 15 (8), 2064. https://doi.org/10.3390/rs15082064.

Heinrich, J., Hoelscher, B., Frye, C., et al., 2002. Improved air quality and reduced respiratory symptoms in Germany. Epidemiology 13 (4), 394–401. https://doi.org/10.1097/01.EDE.0000016977.59359.B6.

Hersbach, H., et al., 2020. ERA5 global reanalysis. Q. J. R. Meteorol. Soc. 146, 1999–2049. https://doi.org/10.1002/qj.3803.

Hou, Y., Wang, Q., Tan, T., 2025. Drivers of PM2.5 pollution using interpretable ML. Waste Manag. 192, 114–124. https://doi.org/10.1016/j.wasman.2024.11.025.

Houdou, A., El Badisy, I., Khomsi, K., et al., 2024. Interpretable ML for air pollution forecasting. Aerosol Air Qual. Res. 24, 230151. https://doi.org/10.4209/aaqr.230151.

Huete, A., et al., 2002. Radiometric performance of MODIS vegetation indices. Rem. Sens. Environ. 83, 195–213. https://doi.org/10.1016/S0034-4257(02)00096-2.

Im, U., Ye, Z., Schuhen, N., et al., 2025. Europe will struggle to meet new WHO guidelines. npj Clean Air 1, 13. https://doi.org/10.1038/s44407-025-00013-w.

Janhäll, S., 2015. Urban vegetation and particle pollution review. Atmos. Environ. 105, 130–137. https://doi.org/10.1016/j.atmosenv.2015.01.052.

Karthick, K., et al., 2024. ML for AQI forecasting in sustainable cities. Earth Science Informatics 17, 3733–3748. https://doi.org/10.1007/s12145-024-01382-8.

Kessinger, S., Minkos, A., Feugenspan, S., 2025. Luftqualität 2024: Vorläufige Auswertung. Umweltbundesamt.

Lange, K., et al., 2023. Validation of Sentinel-5P TROPOMI NO_2 using airborne DOAS. Atmos. Meas. Tech. 16, 1357–1382. https://doi.org/10.5194/amt-16-1357-2023.
Larssen, S., Sluyter, R., Helmis, C., 1999. Criteria for EUROAIRNET. European Environment Agency.
Liu, X., et al., 2021. Air pollution in Germany 2008–2018. Environ. Pollut. 276, 116732. https://doi.org/10.1016/j.envpol.2021.116732.
Long, S., et al., 2022. Estimating NO_2 over China using TROPOMI and ML. Atmos. Environ. 289, 119310. https://doi.org/10.1016/j.atmosenv.2022.119310.
Lolli, S., 2025. Review: urban PM2.5 monitoring and ML. Urban Clim. 63, 102566. https://doi.org/10.1016/j.uclim.2025.102566.
Lyapustin, A., Wang, Y., 2018. MODIS C6 MAIAC algorithm. Remote Sens. 10, 186. https://doi.org/10.3390/rs10020186.
Mamić, L., Gašparović, M., Kaplan, G., 2023. PM2.5/PM10 prediction using open-source EO data. Environ. Monit. Assess. 195 (6), 644. https://doi.org/10.1007/s10661-023-11212-x.
Meijer, J.R., Huijbregts, M.A.J., Schotten, C.G.J., Schipper, A.M., 2018. Global patterns of current and future road infrastructure. Environ. Res. Lett. 13–64006. Data is available at www.globio.info.
Muthukumar, P., et al., 2022. Deep learning for PM2.5 prediction using satellite big data. Air Qual. Atmos. Health 15, 1221–1234. https://doi.org/10.1007/s11869-021-01126-3.
Muñoz-Sabater, J., et al., 2021. ERA5-Land reanalysis. Earth Syst. Sci. Data 13, 4349–4383. https://doi.org/10.5194/essd-13-4349-2021.
Ochege, F.U., et al., 2025. Uncertainty of ML quasi-observations of evapotranspiration. J. Hydrol.: Reg. Stud. 62, 102849. https://doi.org/10.1016/j.ejrh.2025.102849.
OECD, 2023. Environmental Performance Reviews: Germany 2023. https://doi.org/10.1787/f26da7da-en.
Özüpak, Y., Alpsalaz, F., Aslan, E., 2025. Air quality forecasting with ML. Water, Air, Soil Pollut. 236, 464. https://doi.org/10.1007/s11270-025-08122-8.
Pedregosa, F., et al., 2011. Scikit-learn: machine learning in Python. J. Mach. Learn. Res. 12, 2825–2830.
Petetin, H., et al., 2020. Meteorology-normalized COVID-19 NO_2 impacts in Spain. Atmos. Chem. Phys. 20, 11119–11141. https://doi.org/10.5194/acp-20-11119-2020.
Pietikäinen, J.-P., et al., 2015. Emission reductions and aerosol radiative effects. Atmos. Chem. Phys. 15, 5501–5519. https://doi.org/10.5194/acp-15-5501-2015.
Rackow, B., König, H.-H., Wall, M., Konnopka, C., 2025. Interaction of air pollution, weather and health. Sci. Total Environ. 996, 180080. https://doi.org/10.1016/j.scitotenv.2025.180080.
Schatke, M., Meier, F., Schröder, B., Weber, S., 2022. COVID-19 lockdown impacts on NO_2 and PM10 in Berlin. Atmos. Environ. 290, 119372. https://doi.org/10.1016/j.atmosenv.2022.119372.
Schneider, R., et al., 2020. Satellite-based ML PM2.5 model for Great Britain. Remote Sens. 12, 3803. https://doi.org/10.3390/rs12223803.
Shetty, S., 2024. Estimating surface NO_2 in Europe using TROPOMI and ML. Rem. Sens. Environ. 312, 114321. https://doi.org/10.1016/j.rse.2024.114321.
UBA, 2024. Nationale Trendtabellen Für Die Deutsche Berichterstattung. https://www.umweltbundesamt.de/dokument/nationale-trendtabellen-fuer-die-deutsche-4.
UBA, 2025. Population-weighted particulate matter exposure ($PM_{2.5}$). https://www.umweltbundesamt.de/en/indicator-population-weighted-particulate-matter.
van Geffen, J., et al., 2022. TROPOMI NO_2 algorithm theoretical basis. Atmos. Meas. Tech. 15, 2037–2065. https://doi.org/10.5194/amt-15-2037-2022.
Vedrí, J., et al., 2025. Empirical methods for surface air temperature from satellites. Int. J. Appl. Earth Obs. Geoinf. 136, 104380. https://doi.org/10.1016/j.jag.2025.104380.
Venter, Z.S., et al., 2020. Hyperlocal mapping of urban air temperature. Rem. Sens. Environ. 242, 111791. https://doi.org/10.1016/j.rse.2020.111791.
Virta, H., Ialongo, I., Szeląg, M., Eskes, H., 2023. Surface NO_2 estimates from Sentinel-5P in Finland. Atmos. Environ. 312, 119989. https://doi.org/10.1016/j.atmosenv.2023.119989.
Wadoux, A.M.J.-C., Heuvelink, G.B.M., de Bruin, S., Brus, D.J., 2021. Why spatial cross-validation is not the right way to evaluate map accuracy. Ecol. Model. 457, 109692. https://doi.org/10.1016/j.ecolmodel.2021.109692.
Wang, Y., et al., 2025. Combined PM2.5, O_3, NO_2 exposure and health risks in China. Sci. Total Environ. 958, 178103. https://doi.org/10.1016/j.scitotenv.2024.178103.
WHO, 2021. WHO Global Air Quality Guidelines.
WHO, 2024. Ambient Outdoor Air Pollution [Fact sheet].
World Health Organization, 2025. Types of Pollutants.
Wang, Q., Feng, H., Feng, H., et al., 2021. The impacts of road traffic on urban air quality in Jinan based GWR and remote sensing. Sci. Rep. 11, 15512. https://doi.org/10.1038/s41598-021-94159-8.
Wurm, M., Erbertseder, T., Weigand, M., Taubenböck, H., 2025. Global scaling of urban air quality. PLoS One 20 (10), e0333902. https://doi.org/10.1371/journal.pone.0333902.
Yenkikar, A., Mishra, V.P., Bali, M., Ara, T., 2025. Explainable forecasting of AQI using hybrid RF-ARIMA. MethodsX 15, 103517. https://doi.org/10.1016/j.mex.2025.103517.
Zhang, T., et al., 2021. Satellite-based PM2.5 estimation using gradient boosting. Chemosphere 268, 128801. https://doi.org/10.1016/j.chemosphere.2020.128801.
Zhang, Z., et al., 2018. National LUR model for PM in China. Atmos. Environ. 192, 48–54. https://doi.org/10.1016/j.atmosenv.2018.08.046.
Zheng, C., et al., 2017. Factors influencing PM2.5–AOD relationship in Beijing. Atmos. Chem. Phys. 17, 13473–13489. https://doi.org/10.5194/acp-17-13473-2017.
Zheng, Z., et al., 2023. AutoML for evaluating trace gas information for PM2.5 estimation. J. Adv. Model. Earth Syst. 15. https://doi.org/10.1029/2022MS003099 e2022MS003099.
Stratoulias, D., Nuthammachot, N., Dejchanchaiwong, R., Tekasakul, P., & Carmichael, G. R. (2024). Recent Developments in Satellite Remote Sensing for Air Pollution Surveillance in Support of Sustainable Development Goals. Remote Sensing, 16(16), 2932. https://doi.org/10.3390/rs16162932Stratoulias, D., et al., 2024. Satellite RS for air pollution surveillance. Remote Sens. 16 (16), 2932. doi:10.3390/rs16162932.